ELSEVIER

Journal of Nuclear Materials 266–269 (1999) 1084–1090

journal of nuclear materials

Noble gas impurity balance and exhaust model for DIII-D and JET [1]

D.L. Hillis [a,*], J. Hogan [a], M. von Hellermann [b], J. Ehrenberg [b], L. Horton [b], R. König [b], P. Morgan [b], G. Saibene [b], M.R. Wade [a]

[a] *Oak Ridge National Laboratory, Fusion Energy Division, P.O.Box 2009, Oak Ridge, TN 37831, USA*
[b] *JET Joint Undertaking, Abingdon, Oxon OX14 3EA, UK*

Abstract

Experiments to study the exhaust of noble gases (helium and neon) with cryopumping in DIII-D (Advanced Divertor Program (ADP) configuration) and in JET (Mk1 configuration) found significant differences in the global exhaust rate of helium, while efficient neon exhaust was observed in both machines. An attempt to better understand the basic processes governing the exhaust of noble gases in ELMy H-mode with cryopumping has been undertaken. Since divertor geometries investigated in the DIII-D and in the JET cases have significant differences, a comparative modeling study has been undertaken using the MIST core impurity transport code and the b2.5 time-independent divertor transport code. Photodiode measurements are used to determine ELM frequency, and charge-exchange recombination (CER) measurements are compared with the MIST ELM model to evaluate transport coefficients in the core plasma. A significant reduction in the anomalous diffusivities is found for the non-ELM component of radial transport without the need for a pinch velocity, and the model provides a more coherent description than the conventional ELM-averaged approach. Sensitivity to boundary conditions has been studied through establishment of a database of divertor enrichment cases using b2.5.

Keywords: DIII-D; JET; ELM; Helium exhaust; Neon; Transport

1. Introduction

The particle balance for noble gases in ELMy H-mode is of fundamental interest because of the need to exhaust helium in a reactor and of operational interest since injection of non-reacting gases (neon, argon and krypton) is proposed to produce a highly radiative divertor and thereby reduce the heat flux to the graphite divertor tiles [1]. The suitability of H-mode confinement for reactors relies on the observed beneficial effect of ELMs in maintaining quasi-steady densities of both the working gas and the impurities. While ELMy H-mode energy and particle confinement have been found to be compatible with next-step reactor requirements in many machines, (e.g., ITER) [2], recent observation of greatly enhanced heat fluxes during 'type-I' ELMs raises doubts [3,4]. Thus, a better quantitative description of the trade-off between the ELM amplitude needed for effective particle exhaust and a tolerable maximum heat flux is required.

Previous experiments on the exhaust of helium and neon with cryopumping in DIII-D [Lower Single Null (LSN) ADP configuration] and in JET (LSN Mk1 configuration) found significant differences in the global exhaust rate of helium, while efficient neon exhaust was observed in both machines [2,5–7]. Experiments were done in H-mode with 'giant' or 'type-I' ELMs. Estimates [8] show that helium ions must be removed within 7–15 energy confinement times to maintain continuous reactor operation ($\tau^*_{He}/\tau_E \approx 7$–15). Utilizing argon frost pumping (a 10 μm argon frost layer) of helium on DIII-

* Corresponding author. Tel.: +1 423 576 3739; fax: +1 423 576 7926; e-mail: hillisdl@ornl.gov.

[1] Research sponsored in part by the US Department of Energy, under contract number DE-AC05-96OR22464 with Lockheed Martin Energy Research Corporation.

0022-3115/99/$ – see front matter
PII: S0022-3115(98)00563-7

D a value of $\tau^*_{He}/\tau_E \approx 8$ [5] was achieved, which is encouraging for a future fusion reactor. Utilizing a similar 10 μm argon frost layer on JET in the Mk1 divertor, a value of $\tau^*_{He}/\tau_E \approx 15$–20 was obtained [6]. The observed differences for helium exhaust were ascribed to differences in the application of the argon frost technique [9] and to the injection of deuterium and helium to deduce the helium pumping speed prior to the JET experiments. This substantially reduced the helium pumping and spoiled/"poisoned" the argon frost layer for providing high efficiency helium pumping. Neon is readily pumped by the cryopumps of both the JET and DIII-D pumping systems. Subsequent experiments with D_2 injection in DIII-D have shown that neon divertor enrichment is greater than that of helium, and that both can be enhanced with an induced D^+ flow in the scrape-off layer [10,11].

This paper examines the core, scrape-off layer and divertor processes governing helium and neon exhaust to identify similarities and differences. Since the divertor geometries in the cases studied (DIII-D ADP and JET Mk1) are significantly different, a comparative modeling study has been employed to relate exhaust processes in these two experiments. The processes considered are: ELM effects on core transport and enrichment, relative effect of wall reflection coefficients for helium and neon in providing effective exhaust, and device-specific exhaust effects: argon-frost poisoning (for JET Mk1). The modeling components are: time-dependent MIST core radial impurity transport code [12], the b2.5 divertor code [13,14], and the B2-Eirene code system [15,16]. Attention is drawn to previous analysis of these processes in JET discharges using EDGE2D, CHEAP-SANCO, NIMBUS, and other codes [17,18].

2. ELM effects on core transport

In the MIST ELM model [19], an ELM event is modeled as the expulsion of a specified fraction of all the k charge-state densities, $A_{ELM}\ n_k(\rho,t)$, for a normalized radius $\rho > \rho_{ELM}$. A_{ELM} is the expulsion fraction, ρ_{ELM} is the radius where ELMs affect the particle transport, and $n_k(\rho,t)$ is the density of the impurity species. This approach differs from previous models [20,21] in that the ELM is treated as an instantaneous MHD instability, rather than as an extended period of high (L-mode or hybrid) diffusivity. An extended period of high recycling does occur in this model, but with a duration and magnitude governed by the system exhaust and quiescent transport parameters, rather than by an ad-hoc enhanced ELM diffusivity. The times of ELM events (frequency, f_{ELM}) are determined by the measured time histories of the D_α signals. The expulsion fraction is not determined by the D_α signal, and thus both A_{ELM} and ρ_{ELM} become fitting parameters, replacing the ad hoc time dependent variation in the anomalous diffusivity, D_A, and in the pinch velocity, V_p. As an example of the application of the MIST ELM model, Fig. 1 shows the evolution of the neon density in DIII-D (shot 86944) in which neon was continuously injected at an increasing rate throughout the discharge. This increasing neon injection rate causes the large rise in the neon density toward the end of the discharge, as well as producing a change in f_{ELM} from 55 Hz down to 10 Hz starting at $t \sim 2.75$ s. With the ELM model, the Ne XI density measured by CER during this transition is fit with a

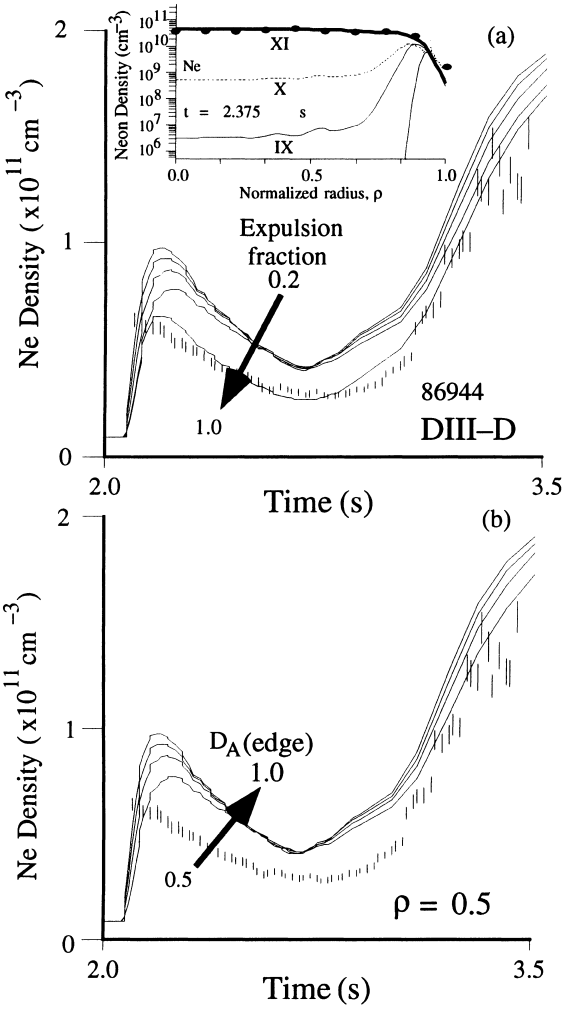

Fig. 1. Comparison of results from MIST ELM model (solid lines) with measured NeXI density (data points) at $\rho = 0.5$ versus time for DIII-D shot 86944. During the shot the ELM frequency varies from 55 Hz to 10 Hz; (a) A variation of the assumed expulsion fraction due to ELMs in the model with $D_A(\text{edge}) = 0.7$ m^2/s and $\rho_{ELM} = 0.8$; (b) A variation of D_A(edge) is shown with the expulsion fraction = 0.2 and $\rho_{ELM} = 0.8$. The inset in (a) shows a typical fit to the neon density radial profile.

time-independent anomalous diffusivity profile [D_A(core) = 0.10 m^2/s and D_A(edge) varied for the best fit] and with $\rho_{ELM} = 0.8$, while f_{ELM} is determined from D_α, and A_{ELM} is selected for each ELM event between 0.3 and 0.6. Fig. 1(a) shows results from the model when the assumed ELM expulsion fraction for neon is varied from 20% to 100% and D_A(edge) = 0.7 m^2/s; likewise, Fig. 1(b) shows a variation of the anomalous diffusivity D_A(edge) from 0.5 to 1.0 m^2/s at a fixed ELM expulsion fraction of 0.2 and a fixed D_A(core) = 0.10 m^2/s. Without the ELM model the transition must be modeled by varying D_A, while the fit in Fig. 1 was obtained with a fixed D_A profile (edge value = 0.7 m^2/s). Best fits are obtained with $D_A = 0.7$ m^2/s, $A_{ELM} \approx 0.5$, and $\rho_{ELM} = 0.8$ using a pinch coefficient, $C_v = 0$, or pinch velocity, $V_p = 0$, in contrast to earlier results for helium, in which $C_v = 1$ was found to be optimum. These values of D_A and A_{ELM} are not unique and other combinations might work equally well. These quantities could be determined experimentally if higher time resolution CER measurements (integration times $\sim$<0.5 ms) were available, but currently they are fitting parameters. A non-zero inward pinch term cannot be ruled out by comparison of the modeling results with the data, but best fits were found for $C_v = 0$. The anomalous diffusivities which result from the MIST ELM model are typically a factor of 3 lower than the diffusivities inferred from the conventional time-averaged analysis, which includes ELM effects as part of the anomalous diffusivity. For core modeling, the effective global recycling coefficient is taken to be 0.96 for neon, as determined by fits to the pumping decay after impurity injection.

For comparison, the ELM model has been applied to model 'type-I' ELM behavior in JET helium and neon exhaust experiments for the Mk1 configuration. In Fig. 2(a)–(c) the time dependence of D_α, carbon, beryllium, and helium edge impurity light is shown for a typical helium case without argon frosting of the cryopump (pulse 30725). The strike point recycling light for each of the impurities shown in Fig. 2(a)–(c) exhibits a similar behavior. These regular 'type-I' ELMs exhibit a cyclic behavior which allows us to analyze intra-ELM behavior. The D_α, carbon, and edge helium signals are shown in Fig. 2(d)–(f) where the individual ELM events have each been remapped onto a single characteristic cycle time, which starts with the beginning of the ELM event. While the D_α and impurity signals are correlated, the response to ELM events differs, reflecting the differences in recycling properties of the species. The carbon and beryllium behavior differs from that of the

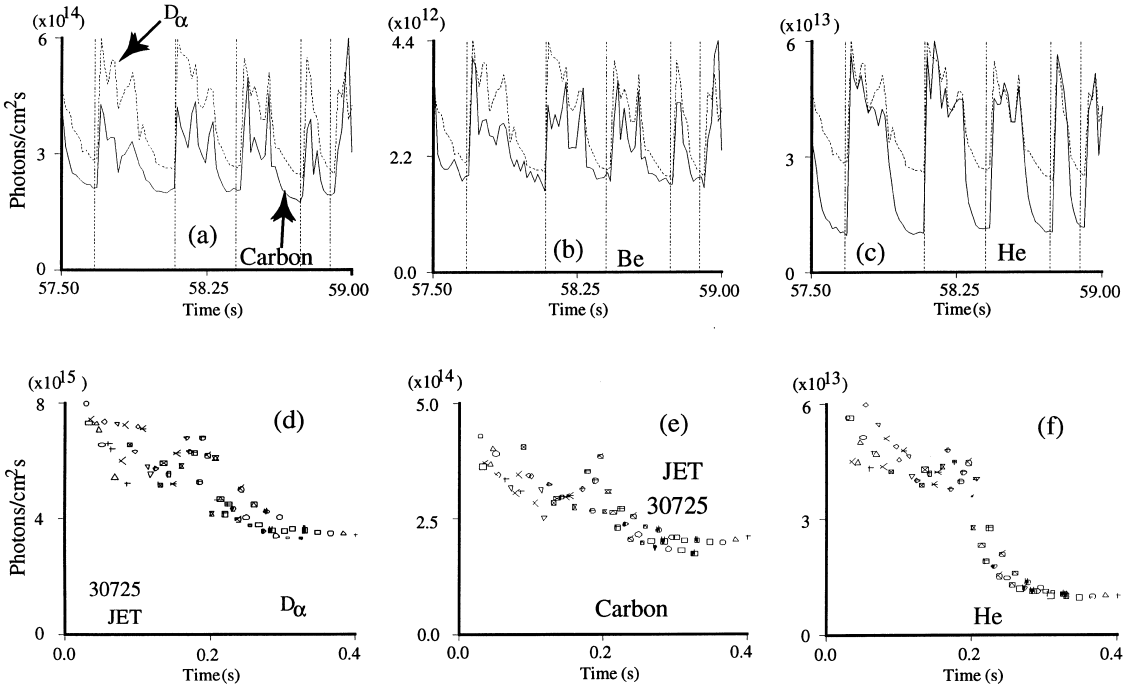

Fig. 2. Measured strike point light for (a) D_α and carbon, (b) beryllium, and (c) helium for JET pulse 30725. The D_α signal (dotted line) is compared with the impurity signals in (a)–(c). The repetitive behavior during the four giant ELMs allows the mapping of the periodic time behavior onto a common time axis (d)–(f), which is given by the first ELM event. (d) Shows the D_α behavior for the four ELM cycles in (a), (e) shows the evolution of carbon during this cycle, and (f) shows the same for helium. The different symbols in (d)–(f) correspond to each of the four individual ELM events.

extrinsic impurities (helium or neon) and this allows us to use MIST modeling of the carbon and beryllium time dependence to establish the ELM-model parameters A_{ELM} and ρ_{ELM}. These ELM parameters are then used for the simulation of the extrinsic injected impurities, either helium or neon. Fig. 3(a) compares the evolution of the helium density measured via CER spectroscopy with (solid line) and without (dashed line) the model for ELM impurity expulsion in JET (shot 30725), while Fig. 3(b) shows the neon evolution compared with the MIST ELM model (shot 32778). For both helium and neon, best fits are obtained using a pinch coefficient, $C_v = 0$. The edge diffusivity which results from the MIST ELM modeling yields $D_A = 1.2$ m^2/s with $A_{ELM} \approx 0.5$ and $\rho_{ELM} = 0.8$; whereas, a value of $D_A \approx 4$ m^2/s is needed to describe the helium density evolution found in Fig. 3(a) if the ELM model is not used. From the modeling of these helium and neon experiments on DIII-D and JET, the value of D_A which is obtained by explicitly treating the ELMs, is typically a factor of ~3 lower than the diffusivities inferred from the conventional time-averaged analysis. For both DIII-D and JET, utilizing this ELM MIST model a time independent $D_A \approx 1.0$ m^2/s describes the data and no inward pinch term is required. These smaller values for D_A are more in line with those expected from neoclassical theory, but a more detailed accounting of the core transport (comparison with neoclassical rates), SOL transport (with ELM effects), and divertor plenum impurity balance would also require simultaneous high time- and space-resolution diagnostic measurements, which currently are not available. In this analysis D_A and A_{ELM} are fitting parameters because high time-resolution diagnostic measurements of the impurity components are not available and other combinations of these parameters may give similar fits to the data. The analysis presented here provides a direct and simple model for treating the ELM expulsion of impurities and provides a useful method for evaluating impurity transport in EL-Ming H-mode discharges.

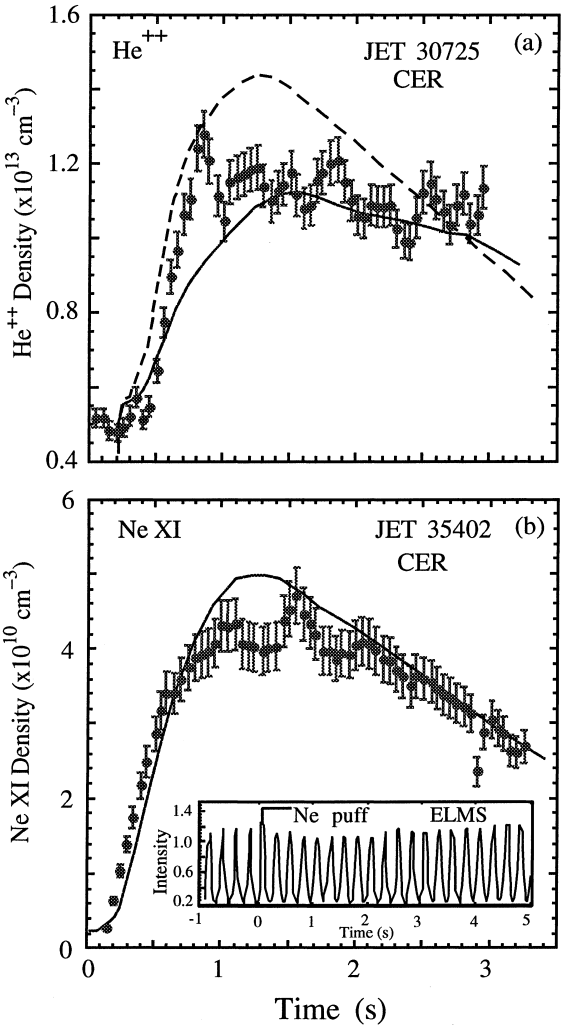

Fig. 3. (a) Comparison of MIST evolution with (solid line) and without (dashed line) the ELM model for helium injection in JET pulse 30725, without argon frost. $D_A = 1.2$ m^2/s for solid curve and $D_A = 3.6$ m^2/s for the dashed curve; (b) Comparison of MIST ELM model (solid line) for neon injection in JET pulse 35402 with 4 Hz giant ELMs. $D_A = 1.2$ m^2/s for the solid curve. The insert shows the ELM activity.

3. Divertor enrichment

The retention of impurities, i (helium or neon) in the divertor is often characterized by the divertor enrichment, η^i_{Div}, and the divertor compression, C^i_{Div} parameters. Here the divertor enrichment is defined as the ratio of helium (neon) concentration at the midplane separatrix to the concentration at the divertor separatrix $\eta^i_{Div} \equiv K_i(\text{div})/K_i(\text{mid})$ and the divertor concentration $K_i = n_i/n_e$. The divertor compression is given by $C^i_{Div} \equiv n_{He}(\text{div})/n_{He}(\text{mid})$, where $n_{He}(\text{div})$ is the helium density in the divertor and $n_{He}(\text{mid})$ is the helium density at the midplane separatrix. More efficient exhaust of neon observed in JET Mk1 experiments relative to helium is consistent with previous observations in DIII-D and ASDEX-Upgrade [10,22]. The pumping plenum concentrations were measured in the latter experiments via a modified Penning gauge, and higher neon compression was observed relative to helium. The JET Penning gauge system for helium and neon measurements in the sub-divertor was not yet installed during the discharges discussed here; therefore, the b2.5 code has been used to estimate the relative divertor concentrations for comparison with DIII-D. Experimental measurements of core plasma parameters, helium and neon density profiles from CER, as well as divertor

measurements (Langmuir probe n_e and T_e profiles and divertor spectroscopy of D, Ne, and He) are utilized as input to b2.5. The b2.5 model is an enhanced version of the b2 code which treats the role of fast reflected particles and plenum-induced gas sources. The particle and energy reflection coefficients derived from TRIM simulations [23] are used to determine the fraction of particles striking the divertor plate which undergo direct reflection (R_N) and the fraction of the emitted energy which is carried by the reflected particles, R_E. The remainder of the particles (unity recycling for non-argon frost cases) are emitted with thermal energies. The code has been run in 5 (deuterium and helium) and 13 (deuterium and neon) species versions. Radial diffusivities are the same as the edge values for the MIST modeling: $D_A = 1.2$ m^2/s and $V_p = 0$. A description of the particle sources from the divertor plate recycling, as well as deuterium and impurity gas injection from the midplane and divertor is included. The STRAHL database [24] is used in the helium/neon comparisons.

Previous comparisons of helium enrichment [10] with that of other non-reacting gases (neon and argon) have explained the observed higher enrichment of neon (and argon) relative to helium by stressing the differences in ionization potential: a longer mean free path for recycled helium atoms leads to a first ionization outside the region of strong deuterium ionization near the divertor plate. Thus an increased D^+ flow in that region is ineffective in producing high enrichment.

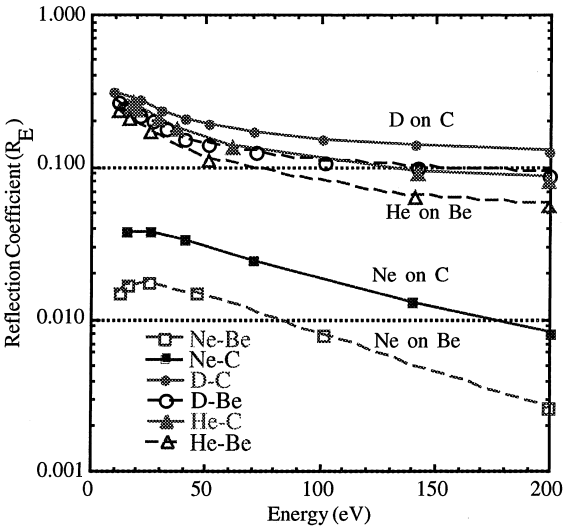

Fig. 4. Comparison of the energy reflection coefficients for deuterium, helium, and neon incident on carbon and beryllium for an assumed incidence angle of 45°. While deuterium and helium have similar values, energy reflection for neon is at least 10 times lower than either of these. The pulses considered here were conducted with both beryllium coated carbon tiles and beryllium tiles.

However, modeling of these JET Mk1 experiments suggests an equally important effect of fast reflected atoms in reducing the helium enrichment. JET Mk1 experiments were conducted with beryllium coated carbon surfaces. Fig. 4 shows the variation in energy reflection

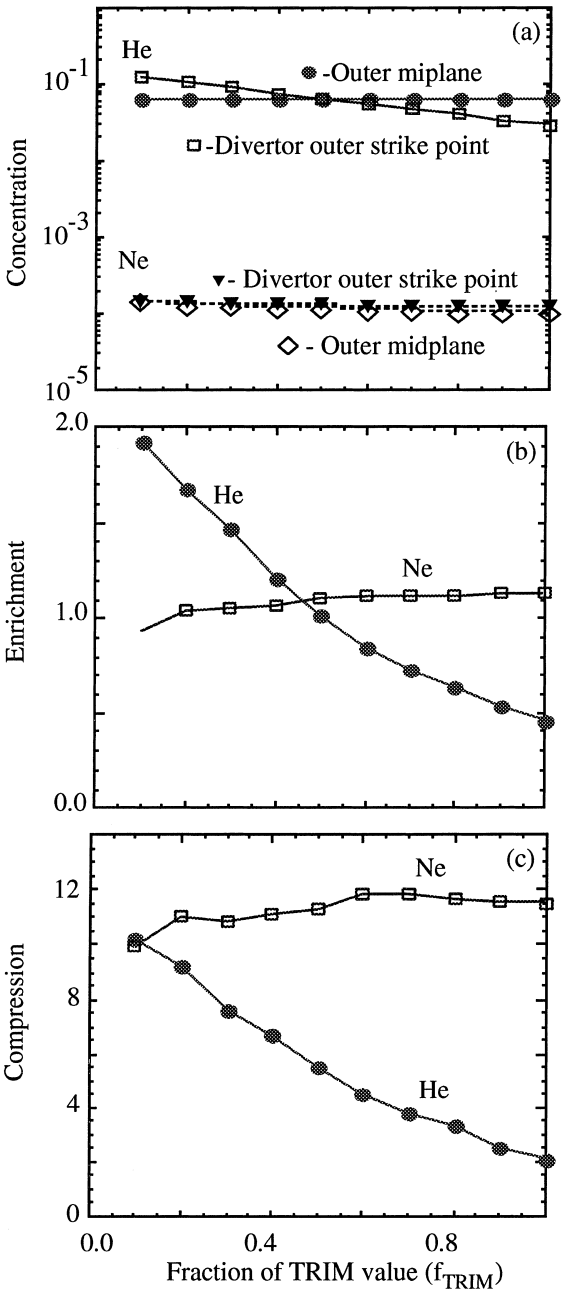

Fig. 5. Results of a b2.5 survey for conditions of JET pulse 33994 (helium) and 32778 (neon) showing the sensitivity of divertor and midplane helium (neon) concentrations, enrichment, and compression to the assumed fraction of the TRIM value, f_{TRIM}.

coefficients (TRIM values) expected for helium and neon incident on carbon and beryllium for the energy range observed in these experiments [from divertor probes $T_e \approx 30$–60 eV, with corresponding impact energy ($3\langle Z\rangle kT_e + 2\ T_i \leqslant 200$ eV)]. Generally, smaller values are expected, due to the surface roughness of actual divertor plates and also due to the incomplete coverage of carbon with beryllium. Fig. 5 shows the results from the b2.5 calculations when the assumed energy reflection coefficient (R_E) is varied with respect to the TRIM value for helium (pulse 33994) and neon (pulse 32778) by varying f_{TRIM} from 0.1 to 1.0 through the relation $R_E = f_{TRIM} \cdot R_E(\text{TRIM})$. From Fig. 5 the helium compression is ~2 and for neon ~12 at the TRIM values ($f_{TRIM} = 1.0$), while the helium enrichment is ~0.5 and for neon enrichment ~1.1. As the energy reflection coefficient is reduced for helium ($f_{TRIM} < 1.0$) the compression rises by a factor ~5, whereas, for neon the compression remains ~12. Because of the low value for the direct reflection coefficient ($R \sim 0.01$) for neon, most of the recycled neon emerges at thermal energies and with its larger mass the neon residence time in the vacuum plenum will be ~300 times longer than that for deuterium. Some of the reported discrepancies [10,25] in neon inventory during injection experiments may be due to this effect alone. Due to variations in the roughness of the divertor tiles f_{TRIM} is probably between 0.5 and 1.0. Table 1 shows the modeled enrichment and compression values for the JET Mk1 divertor for helium and neon compared with those measured on DIII-D and ASDEX. Very good agreement is observed between the two cases. Typically, the helium and neon enrichment are: $\eta_{Div}^{He} \approx 0.9$, $\eta_{Div}^{Ne} \approx 1.1$, respectively; while the helium and neon compressions are found to be: $C_{Div}^{He} \approx 3$ and $C_{Div}^{Ne} \approx 11$, respectively. Values found in parentheses in Table 1 for DIII-D are enrichment and compression values with an induced scrape-off-layer flow [10]. It should be noted that these b2.5 calculations are time independent and the enrichment and compression factors are most representative for the time period between ELMs. During periods of ELM activity the enrichment may vary by large factors. Recent preliminary measurements [26] on the JET Mk2 divertor in L-mode indicate that the helium enrichment is ~0.8–1.1, also providing confidence in the values reported here for Mk1 utilizing the b2.5 modeling.

4. Conclusions

Comparison of DIII-D and JET Mk1 helium and neon exhaust experiments has been made with respect to core transport (ELM effects) and divertor enrichment. The experiments are quite different due to significant differences in divertor geometry and the size of the tokamak. A comparative modeling study finds similar reductions in inferred edge diffusivity when an ELM instability model is applied. The ELM model replaces the usual ad hoc ELM-averaged diffusivity with new parameters describing the fraction of impurity density which is expelled during an ELM event and the radius over which the ELM is effective in purging impurities. For both DIII-D and JET, the edge diffusivity, $D_A \approx 4$ m^2/s, is found if ELM effects are not included in the model; whereas, $D_A \approx 1.0$ m^2/s if the ELMs are explicitly included in the model without the need for a time varying D_A or pinch velocity ($V_p = 0$). Since the inferred core radial diffusivities are reduced with respect to ELM-averaged models, a closer comparison with neoclassical theory for the diffusivity may be warranted. Utilizing the b2.5 code and experimentally measured core and divertor plasma properties, the divertor enrichment and compression in the JET Mk1 configuration were calculated and found to be sensitive to the differences in particle reflectivity between helium and neon. The much lower particle reflection coefficients for neon leads to a larger predicted enrichment, relative to helium. This is consistent with observations that neon is more readily exhausted than helium. Finally, a detailed examination of core transport, exhaust, and divertor enrichment should include the effect of impurity purging during ELM events, which are quite complex. To further investigate the fast time scales of ELM events and the underlying mechanisms for impurity entrainment and compression higher time resolution edge and divertor diagnostics will be required.

Table 1
Comparison of helium and neon enrichment and compression factors in ELMing H-mode discharges for JET(Mk1), JET(Mk2), DIII-D and ASDEX-U

Impurity	JET(Mk1) [a]	JET(Mk2) [26]	DIII-D[10,11]	ASDEX-U[22,25]
Helium enrichment	0.6–1.0	0.8–1.1	0.9 (1.1) [b]	0.3–0.4
Neon enrichment	1.1		1.0–1.2 (1.6–2.3) [b]	
Helium compression	2–4		4.3 (6.1) [b]	3.5(1–3)
Neon compression	11		4.6–7.8 (6.2–14.2) [b]	13

[a] Values based upon b2.5 modeling described in the text.
[b] Values found in experiments with induced flow in the scrape-off layer (see Refs. [10,11]).

References

[1] S.L. Allen et al., J. Nucl. Mater. 196–198 (1992) 804.
[2] J. Hogan et al., J. Nucl. Mater. 241 (1997) 68.
[3] E. Gauthier et al., in: Proceedings of 24th EPS Conference on Controlled Fusion and Plasma Physics, vol. 21A, part 1, Berchtesgaden, Germany, 1997, p. 61.
[4] S. Clement et al., these Proceedings.
[5] M.R. Wade et al., Phys. Rev. Lett. 74 (1995) 2702.
[6] M.G.v. Hellermann et al., in: Proc. 22nd European Conference on Controlled Fusion and Plasma Physics, vol. 19C, part II, Bournemouth, UK, 1995, p. 12.
[7] P.J. Harbour et al., in: Proceedings of 22nd European Conference on Controlled Fusion and Plasma Physics, vol. 19C, part IV, Bournemouth, UK, 1995, p. 465.
[8] D. Reiter et al., Nuclear Fusion 30 (1990) 2141.
[9] G. Saibene et al., in: Proceedings of 22nd European Conference on Controlled Fusion and Plasma Physics, vol. 19C, part II, Bournemouth, UK, 1995, p. 121.
[10] M. Wade et al., Impurity enrichment studies with induced scrape-off-layer flow on DIII-D, Nuclear Fusion, in press.
[11] M.R. Wade et al., these Proceedings.
[12] R.A. Hulse, Nuclear Technology/Fusion 3 (1983) 259.
[13] R. Maingi et al., Nuclear Fusion 34 (1994) 283.
[14] B.J. Braams, NET Report: EUR-FU/XII-80/87/68, 1987.
[15] R. Schneider et al., J. Nucl. Mater. 196–198 (1992) 810.
[16] D. Reiter, Report Juel-2599, Forschungszentrum, Juelich, 1992.
[17] L. Lauro-Taroni et al., Contributions to Plasma Physics 38 (1998) 241.
[18] M. Fichtmueller et al., these Proceedings.
[19] J. Hogan et al., in: Proceedings of the 24th European Physical Society Conference on Controlled Fusion and Plasma Physics, vol. 21A, Berchtesgaden, Germany, 1997, p. 1133.
[20] R. Dux et al., Plas. Phys. Contr. Fusion 38 (1996) 989.
[21] M. O'Mullane et al., in: Proceedings of 22nd EPS Conference on Controlled Fusion and Plasma Physics, vol. III, Bournemouth, UK, 1995, p. 121.
[22] H.S. Bosch et al., J. Nucl. Mater. 241–243 (1997) 82.
[23] W. Eckstein, IPP-Garching Report: IPP 9/217, 1998.
[24] K. Lackner et al., Z. Naturforsch. 37a (1982) 931.
[25] H.-S. Bosch et al., Plasma Phys. Control. Fusion 39 (1997) 1771.
[26] M. Groth et al., in: Proceedings of 25th European Conference on Controlled Fusion and Plasma Physics, 1998 (to be published).